α-Sn phase on Si(111): Spin texture of a two-dimensional Mott state

M. Jäger,[1] C. Brand,[1,*] A. P. Weber,[2,3] M. Fanciulli,[2,3] J. H. Dil,[2,3] H. Pfnür,[1] and C. Tegenkamp[1,4,†]

[1]*Institut für Festkörperphysik, Leibniz Universität Hannover, Appelstrasse 2, 30167 Hannover, Germany*

[2]*Institute of Physics, École Polytechnique Fédérale de Lausanne, 1015 Lausanne, Switzerland*

[3]*Photon Science Division, Paul Scherrer Institut, 5232 Villigen PSI, Switzerland*

[4]*Institut für Physik, Technische Universität Chemnitz, Reichenhainer Str. 70, 09126 Chemnitz, Germany*

(Received 14 August 2018; published 15 October 2018)

The α-Sn reconstruction on Si(111) is a prototype system for a two-dimensional Mott phase. In this study we performed spin-resolved photoemission experiments and analyzed in detail the spin structure of this electronically correlated surface state. The analysis of the spin-integrated bands as well as the spin texture of the surface states along different crystallographic directions provide clear evidence for the formation of collinear antiferromagnetic $(2\sqrt{3} \times \sqrt{3})$ domains, while the Sn reconstruction reveals a $(\sqrt{3} \times \sqrt{3})$ symmetry. The Rashba splitting of the highest occupied Mott state was found to be $\Delta k = 0.05\,\text{Å}^{-1}$, i.e., the α-Sn phase should be termed a weakly spin-orbit coupled Mott system.

DOI: 10.1103/PhysRevB.98.165422

I. INTRODUCTION

The wealth of exotic phenomena, e.g., superconductivity, charge density waves, and spin liquids [1–3], can be greatly explored by two-dimensional (2D) electron gases realized by adsorption of (sub)monolayer structures on semiconducting surfaces. Particularly, the group IV elements with their electronic s^2p^2 configuration display a wide spectrum of correlated phases: For instance, Pb monolayer (ML) structures show pronounced electron-phonon coupling and give rise to charge ordering transitions on Ge(111) [3,4] or Cooper pairing on Si(111) [1,5], while Sn on Si(111) is a prototype Mott system. A coverage of 1/3 ML Sn forms a long-range ordered $(\sqrt{3} \times \sqrt{3})$ reconstruction, the so-called α-Sn phase, with the Sn atoms located at T_4 sites [6,7]. This phase reveals an isostructural metal-insulator transition (MIT) upon cooling below 70 K [8]. Moreover, with ARPES a gap energy of around 200 meV was found [9]. Scanning tunneling spectroscopy (STS) and conductivity measurements indicate that the MIT is driven by strong electron correlations [10,11].

If spin-orbit coupling is effective, the electronic effects are intimately related to magnetic phases [12]. In addition, the frustration of spin-1/2 systems on 2D triangular lattices favors complex spin textures [13,14] and leads to new quantum phenomena, e.g., for densely packed Pb monolayers on vicinal Si(111) surfaces a spin-orbit density wave was found with Fermi nesting between helical states and antiferromagnetic ordering [15]. In contrast, on flat Si(111) the 2D nesting vectors are incommensurate, thus keeping this system rather immune against charge density wave formation and possibly enabling superconducting behavior [5,16].

Compared to Pb, the electronic correlation effects for α-Sn are much stronger due to the smaller orbital size. On the other hand, because of the smaller Z of Sn, the role of spin-orbit coupling just recently came into the focus of research. Theoretical results show that the insulating ground state of α-Sn might be a ferrimagnetic Slater-type insulator via itinerant magnetic order [17,18] or, on account of spin-orbit coupling, a 120°-Néel structure with noncollinear ordering [19]. Based on high resolution photoemission experiments and density functional theory (DFT) [9], a description of the (spin-integrated) spectral function is only possible if row-wise collinear antiferromagnetic order with a $(2\sqrt{3} \times \sqrt{3})$ symmetry at low temperatures is assumed for the Mott state. Indeed, the same symmetry was obtained by recent hybrid DFT calculations but suggesting a Slater-type insulator via band magnetism [17]. Surprisingly, spin-resolved measurements on this system that can give a more detailed insight in the spin ordering are missing up to now.

In this paper we want to elucidate the effect of SOC in a correlated electronic system, and we measured directly the spin components of the surface states in the Mott regime by means of spin- and angle-resolved photoemission (SARPES). The Rashba-type spin splitting is found to be around $0.05\,\text{Å}^{-1}$. Moreover, we measured spin-resolved momentum distribution curves (MDC) along various high symmetry directions giving clear evidence for the $(2\sqrt{3} \times \sqrt{3})$ row-wise collinear antiferromagnetically ordered spin cell, while low energy electron diffraction (LEED) reveals a $(\sqrt{3} \times \sqrt{3})$ symmetry.

II. EXPERIMENTAL DETAILS

Long-range ordered Si(111) surfaces (phosphorous-doped, 0.01 Ω cm) as templates for Sn adsorption were prepared by degassing the samples at 500 °C for several hours and repeated flash annealing to 1150 °C until a sharp (7×7) reconstruction

*Present address: Fakultät für Physik & CENIDE, Universität Duisburg-Essen, Lotharstrasse 1, 47057 Duisburg, Germany.

†christoph.tegenkamp@physik.tu-chemnitz.de

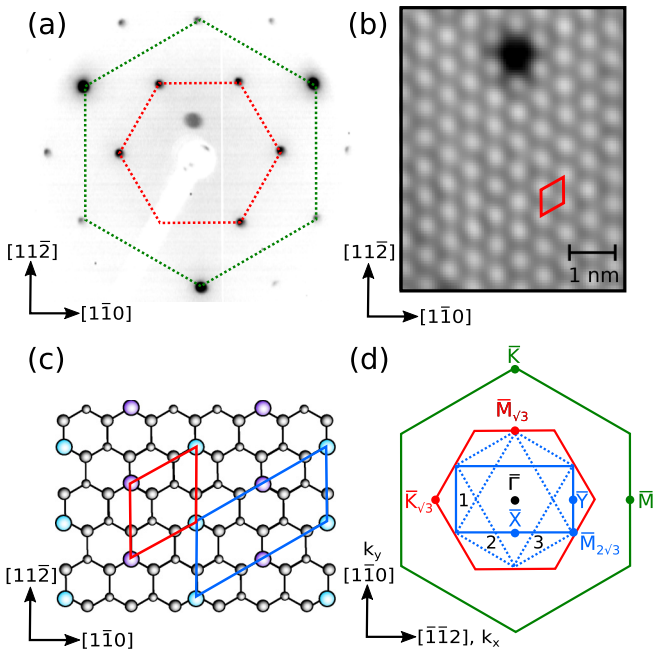

FIG. 1. (a) LEED image of α-Sn taken at an electron energy of 76 eV at a temperature of 40 K. Dashed lines connect the first order diffraction spots of (1×1) (green) and $(\sqrt{3} \times \sqrt{3})$ (red). The feature next to the electron gun stems from a defect on the screen. (b) STM (+1 V, 0.1 nA) image of the α-Sn phase with a vacancy taken at room temperature. (c) Top view of the α-Sn reconstruction on Si(111). Blue and violet circles represent Sn atoms on T_4 adsorption sites with different spin polarizations; Si atoms are gray. Red and blue lines indicate the $(\sqrt{3} \times \sqrt{3})$ and $(2\sqrt{3} \times \sqrt{3})$ unit cell, respectively. (d) SBZs of the (1×1) (green), $(\sqrt{3} \times \sqrt{3})$ (red), and three rotational $(2\sqrt{3} \times \sqrt{3})$ domains (blue). The domain labeled as '1' is referred to as the horizontal domain, while domains '2' and '3' are termed rotated domain structures.

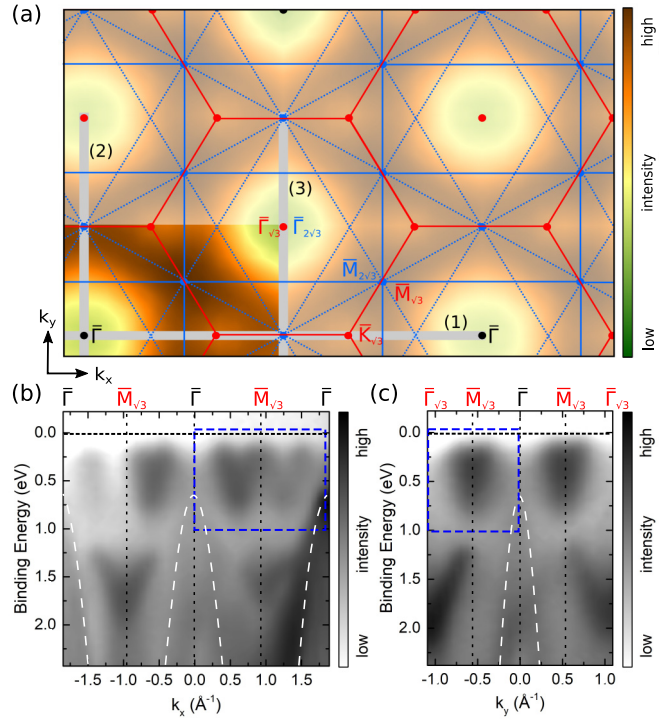

FIG. 2. (a) Extended CEM taken at $E_B = 0.38$ eV. Only the phase space shown in the lower left was measured. The superimposed red and blue lines show the SBZs of the $(\sqrt{3} \times \sqrt{3})$ and of the three rotational domains of $(2\sqrt{3} \times \sqrt{3})$, respectively. Dots symbolize high symmetry points of both structures; gray lines highlight the directions of the (S)ARPES measurements. (b) Band map along the k_x direction (1). (c) Band map along the k_y direction (2). Dashed white curves show the positions of the Si valence band. Details of the band maps within the blue boxes are shown in Fig. 3.

was seen by LEED. Afterwards, 1/3 of a monolayer of Sn was evaporated on the surface while the sample was held at 600 °C. The quality of the α-Sn surface reconstruction with $(\sqrt{3} \times \sqrt{3})$ symmetry was checked afterwards by LEED as shown exemplarily in Fig. 1(a). The diffraction pattern remains unchanged upon cooling down to 40 K with ℓHe. The rate of evaporation was calibrated independently by scanning tunneling microscopy [STM, cf. Fig. 1(b)] experiments.

Spin-resolved and spin-integrated ARPES measurements were performed at the COPHEE end station at the SIS beamline of the Swiss Light Source [20]. Unless otherwise indicated, right-handed circularly polarized light (C^+) with a photon energy of 90 eV was used. The photoemission experiments were carried out at low temperatures (40 K), well below the phase transition temperature of ~70 K. In order to reveal a good signal to noise ratio the (spin-resolved) MDCs were taken at a binding energy of $E_B = 0.38$ eV below the Fermi energy E_F. For spin-integrated ARPES, energy and angular resolution are 25 meV and 0.3°, respectively. In the spin-resolved mode, a resolution of 80 meV and 0.75° can be reached. Details about the experimental setup and the analysis of the spin data are described elsewhere [21].

III. RESULTS AND DISCUSSION

A. Structure of the α-Sn phase

A top view of the α-Sn structure is sketched in Fig. 1(c). The $(\sqrt{3} \times \sqrt{3})$ reconstruction of the Sn atoms, highlighted with red lines, is seen with LEED and STM [cf. Figs. 1(a) and 1(b)] both above and below the transition temperature [8]. If we associate a spin to the Sn atoms, they are ordered in a row-wise collinear antiferromagnetic pattern, and a $(2\sqrt{3} \times \sqrt{3})$ spin unit cell is formed. This unit cell generally exists in three domains rotated by 120° with respect to each other [9]. The corresponding surface Brillouin zones (SBZs) for both reconstructions and their high symmetry points are sketched in Fig. 1(d).

B. Spin-integrated constant energy and band maps

The constant energy map (CEM) of the α-Sn phase, illustrated in Fig. 2(a), was taken at 0.38 eV below the Fermi energy E_F. A surface state with high intensity is observed around the $\bar{M}$ points of the $(\sqrt{3} \times \sqrt{3})$ and two domains of $(2\sqrt{3} \times \sqrt{3})$ unit cells. The local minimum of this dispersing state is located at $\bar{K}_{\sqrt{3}}$. The SBZ boundaries and symmetry points of both reconstructions are superimposed for clarification.

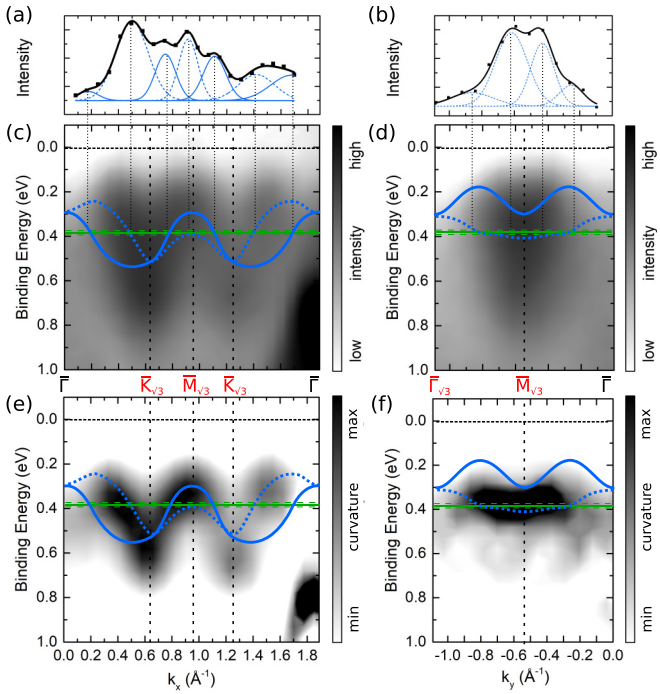

FIG. 3. (a),(b) MDCs along the k_x and k_y directions taken at 380 meV, respectively. (c),(d) Band maps along the k_x and k_y directions. (e),(f) curvature maps of (c) and (d) to highlight details of the band structure. Green lines show the position of the MDCs. Solid and dashed blue curves indicate (spin-degenerate) calculated surface bands from domain 1 and domains 2, 3 of the $(2\sqrt{3} \times \sqrt{3})$ structure, respectively. The band structure was taken from Ref. [17].

Band maps along two high symmetry directions are shown in Figs. 2(b) and 2(c). They clearly reveal the insulating nature of the ground state at low temperature, showing an energy gap of $\Delta E \approx 0.1$ eV with respect to E_F [9]. For better orientation, we marked the valence band maximum of Si.

In order to characterize the surface states in more detail we show in Fig. 3 an enlargement of the region marked by rectangles in Figs. 2(b) and 2(c). Clearly, the surface state along the k_x direction reveals a w shape with minima around 0.6 eV binding energies located at the $\bar{K}_{\sqrt{3}}$ points [cf. Fig. 3(c)]. A pronounced broadening of all surface states is obvious and was also seen in other high resolution ARPES experiments [9]. As we will show in the following, this apparent smearing is rather an effect of the multidomain structure of the $2\sqrt{3} \times \sqrt{3}$ reconstruction and the Rashba-type spin splitting of the surface states.

Figure 3 shows a comparison between our measured MDCs and the band structure based on previous calculations [9,17]. Starting with the k_x direction, there is some intensity in the vicinity of the $\bar{\Gamma}$ point, which can be seen more clearly in the curvature fit of the band map shown in panel (e). This faint feature was observed before, and its position at around 0.4 eV binding energy is indicative for the broken $(\sqrt{3} \times \sqrt{3})$ symmetry [9]. Moreover, the MDC curve shown in Fig. 3(a) reveals a multipeak structure which is visible also in the curvature plot of the data [Fig. 3(e)].

Quantitative agreement for the positions of the multipeak MDC structure with calculations is obtained if contributions of the surface state from different domains are taken into account. The solid and dashed blue curves display (spin-degenerate) surface bands for the horizontal (domain 1) and the rotated domains, respectively. The band structures for the $(2\sqrt{3} \times \sqrt{3})$ reconstruction were taken from Lee *et al.* [17]. Thereby, the dashed curve is the projection of the band structure from two rotated domains and thus should comprise twice as much intensity compared to the band belonging to domain 1. Indeed, this trend is seen in the MDC curve, at least for the first sequence of peaks. The gradual damping of the signal along the k_x direction comes either from a slight azimuthal misalignment of the scan direction, changes in the dipole selection rules with changing incidence angle of light, and/or the physisorption of UHV rest gas. As we will show in the next section, the Rashba-type spin splitting along the k_x direction is approximately five times smaller than the band splitting seen in the MDC, thus already the analysis of the spin-integrated data provides clear evidence for the collinear antiferromagnetic ordering with $(2\sqrt{3} \times \sqrt{3})$ symmetry.

Along the k_y direction the band structure, displayed in Figs. 3(d) and 3(f), consists of two bands as well. In contrast to the k_x direction, the bands disperse less [17]. While the band originating from domain 1 disperses at binding energies between 0.2–0.3 eV, the other band is located between 0.3–0.45 eV. Thus, the MDC taken at $E_B = 0.38$ eV does not comprise any bands from domain 1 but four peaks from domains 2 and 3. Contrary to the k_x direction, the splitting along the k_y direction is mainly due to spin-orbit interaction as we will show in the following. Again, the interpretation of the spin-integrated ARPES data indicates the $(2\sqrt{3} \times \sqrt{3})$ symmetry.

C. Spin-resolved band structure

In order to further investigate the spin-orbit coupling in these surface bands, (spin-integrated) MDCs were taken again at $E_B = 0.38$ eV along k_y [part of the direction is marked by (3) in Fig. 2(a)], but with right (C^+) and left (C^-) circularly polarized light at a photon energy of $h\nu = 44$ eV. Figure 4(a) shows the corresponding band map along the k_y direction. Notably, the Si valence bands are seen here as replica structures around the $\bar{\Gamma}_{\sqrt{3}}$ points, which indicates the long-range ordering of the α-Sn reconstruction.

Both MDCs have roughly the same shape but they show deviations in intensity on the side of the peaks originating from the surface bands. This means that those states show circular dichroism which indicates that spin-orbit interaction plays an important role and the states have to be described by different quantum numbers. A more detailed analysis was done by plotting the difference and fitting the sum of C^+ and C^- spectra in panels (c) and (d), respectively. The helicity dependent photoemission intensity is ascribed to two spin-orbit split states symmetrically shifted around the time-reversal invariant $\bar{M}_{\sqrt{3}}$ points. Within the errors of the measurement, the splitting is identical to the splitting discussed in the context of Fig. 3(b). We will show below that the circular dichroism is most likely a result of Rashba-type spin splitting of the surface states.

In order to quantify further the spin texture of the surface states and to rule out that the dichroitic signal is entirely

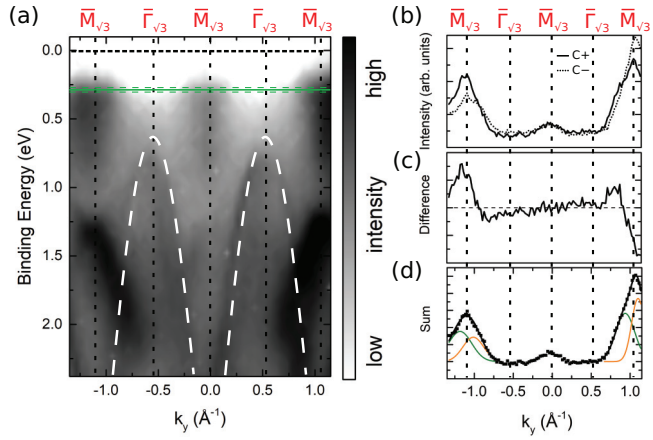

FIG. 4. (a) Band map along the direction denoted by (3) in Fig. 2, where the MDCs were taken. The dashed curves show the $\sqrt{3} \times \sqrt{3}$-replica states of the Si valence bands. (b) MDC curves taken along the k_y direction with C^+ and C^- polarization. (c) and (d) show the difference and sum of the two MDC spectra, respectively.

governed by matrix element effects, we performed SARPES measurements, again at a binding energy of $E_B = 0.38$ eV. Figure 5(a) shows the spin-resolved MDC along the k_x direction. A comparison with the spin-integrated signal shown in Fig. 3(a) yields qualitatively the same shape. The measurement was started this time from the high momentum side, i.e., the gradual drop in intensity is most likely induced by physisorption of residual gas. The three measured spin components, shown in Fig. 5(b), clearly reveal a pronounced in-plane spin polarization of the surface states (nonvanishing S_x, S_y).

A simultaneous description of all four data sets ($S_{x,y,z}$ and total intensity) is achieved only if a peak substructure as

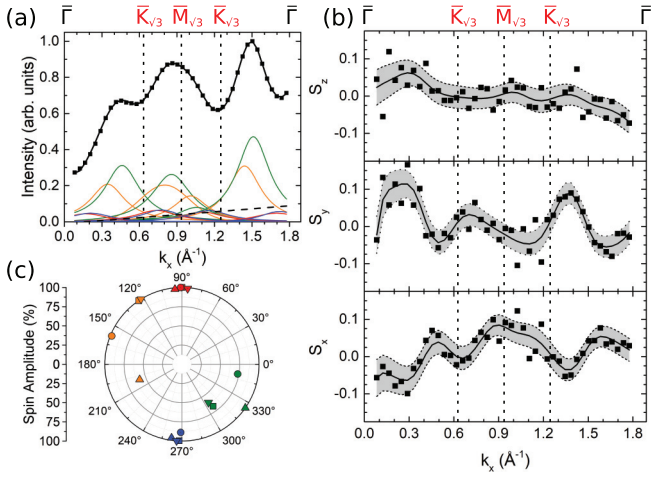

FIG. 5. (a) Spin-resolved MDC along the k_x direction taken at 0.38 eV below E_F. The upper axis shows the high symmetry points [cf. Fig. 1(d)]. (b) Corresponding spin-polarization vectors S_x, S_y, and S_z. The shaded areas represent the uncertainty by simultaneously fitting all four data sets. (c) S_x and S_y spin components of the peaks shown in (a). The 0° and 90° denote the positive x and y directions, respectively.

shown in Fig. 5(a) is considered: First of all, each intensity feature comprises a doublet structure which accounts for the Rashba spitting. The presence of a doublet with reversed spin ordering is partly visible also in the raw data, e.g., from the rapid change of amplitude of the S_y component around 1.5 Å^{-1}. Secondly, the most intense MDC peaks discussed in the context of Fig. 3(a) (dashed lines, rotated domains) are considered by the three intense double peak structures (marked by green and orange lines). Furthermore, the less intense peaks seen in Fig. 3(a) (solid lines, domain 1) were detectable and taken into account by a corresponding sequence of double peaks (red and blue curves). It should be emphasized that a better agreement is obtained if instead of six peaks eight peaks are considered for the rotated domains in Fig. 5(a). Any modeling with less peaks was not able to describe the variations in magnitude of the three spin polarizations satisfyingly. We already pointed out that at the constant energy of 0.38 eV we barely touch the surface bands originating from these domains [cf. dashed lines in Fig. 3(c)]. For the measurements with the Mott detectors, the energy resolution is lower and the larger integration area is most likely the reason for this observation. Based on this initial guess, a satisfying modeling of the experimental spin-resolved data succeeded.

A polar plot of the resulting in-plane spin components S_x and S_y is shown in Fig. 5(c): Indeed, each of the doublet structures reveals de-facto an opposite spin orientation, as expected for conventional Rashba-split states. The splitting is around $\Delta k_x \approx 0.05$ Å^{-1}, which means that the α-Sn phase can be described by a correlated quantum state with weak spin-orbit coupling [12]. Furthermore, the less intense peaks belong to domain 1, in agreement with the assignments done in Figs. 3(a) and 3(c). Consequently, due to the mirror plane of this domain, only S_y spin components are observed for the k_x direction. Contrary, the spin vectors originating from the rotated domains show both S_x and S_y components. The spin texture from these states originates from both domains. Therefore, any imbalance between these two domains will cause a finite S_x component [16]. Nevertheless, the analysis is fully consistent with our conclusions from the previous section and supports the formation of $(2\sqrt{3} \times \sqrt{3})$ domains. The finding of in-plane spin components suggests an in-plane anti-ferromagnetic ordering between the Sn sites. Similar magnetization patterns were reported for Mn/W(110) [22].

Besides the k_x direction, we also measured the spin components of the surface state along the k_y direction (cf. Fig. 6). According to the discussion in the context of Fig. 3(d) the surface state at around 0.38 eV binding energy is formed by states of the rotated domains. A four-peak structure is mandatory for the momentum range in order to describe satisfyingly the MDC intensity and three spin-component data sets. Clearly, the adjacent peaks show an alternating spin structure. However, the apparent larger Rashba splitting of $\Delta k_y \approx 0.2$ Å^{-1} is a result of the intersection of the Mott states from adjacent zones and not an indication of an anisotropic spin texture, as we will show below. If both domains were equally distributed, only the S_x component should show up. The finite value of S_y component reflects the asymmetry

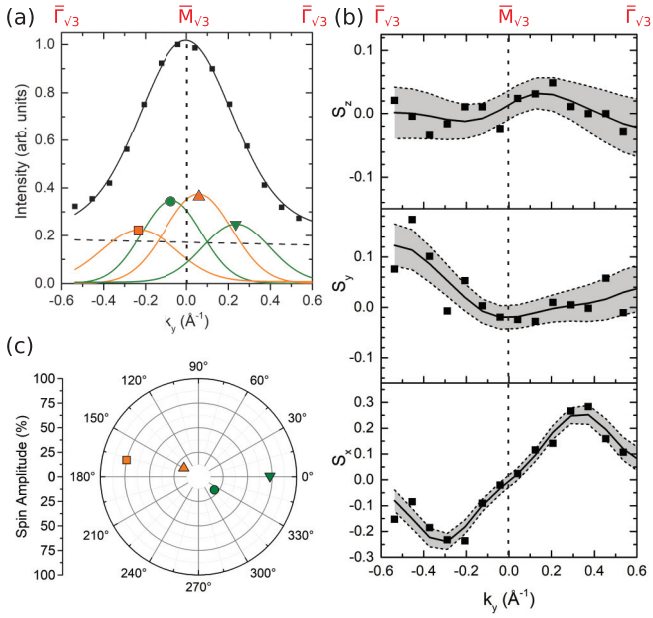

FIG. 6. (a) Spin-resolved MDC along the k_y direction taken at 0.38 eV below E_F. The upper axis shows the high symmetry points of the three domains [cf. direction (3) in Fig. 2(a)]. (b) Corresponding spin-polarization vectors S_x, S_y, and S_z. The shaded areas represent the uncertainty by simultaneously fitting all four data sets. (c) S_x and S_y spin components of the peaks shown in (a).

between these two domains, in accordance with the conclusions drawn above.

D. Model for the spin texture of α-Sn phase

For the spin-ordered $(2\sqrt{3} \times \sqrt{3})$ structure, Lee *et al.* [17] calculated a band structure for one domain containing one only slightly dispersing surface band with a binding energy between approximately 0.1 and 0.5 eV. In accordance with the results in this work concerning the spin-orbit interaction, a Rashba-type spin splitting of $\Delta k \approx 0.05$ Å^{-1} is superimposed in Fig. 7(b) while maintaining spin degeneracy at time-reversal invariant momenta. Consequently, the rectangular SBZ comprises two almost circularly shaped bands around the $\overline{\mathrm{Y}}$ point with opposite spin directions as seen in Fig. 7(a). Along the mirror plane xz in the k_x direction, crossing through $\overline{\Gamma}$ and $\overline{\mathrm{Y}}$, the spin components S_x and S_z are zero and only S_y has a finite value in agreement with our finding.

In Fig. 7(c) all three rotational domains are depicted in an extended zone scheme. The surface bands of different domains overlap each other resulting in a complex electronic structure model. Looking along the k_x direction, i.e., $\overline{\Gamma\mathrm{Y}}$ of the horizontal domain, one finds an alternating spin structure originating either only from domain 1 or an overlap of the surface bands of the two other domains 2 and 3 [numbering refers to Fig. 1(d)]. Along the k_y direction, $\overline{\Gamma\mathrm{X}}$ of domain 1, only bands of domain 2 and 3 appear. The domains are spatially separated and no interaction between the bands of different domains can be expected. However, in measurements, the

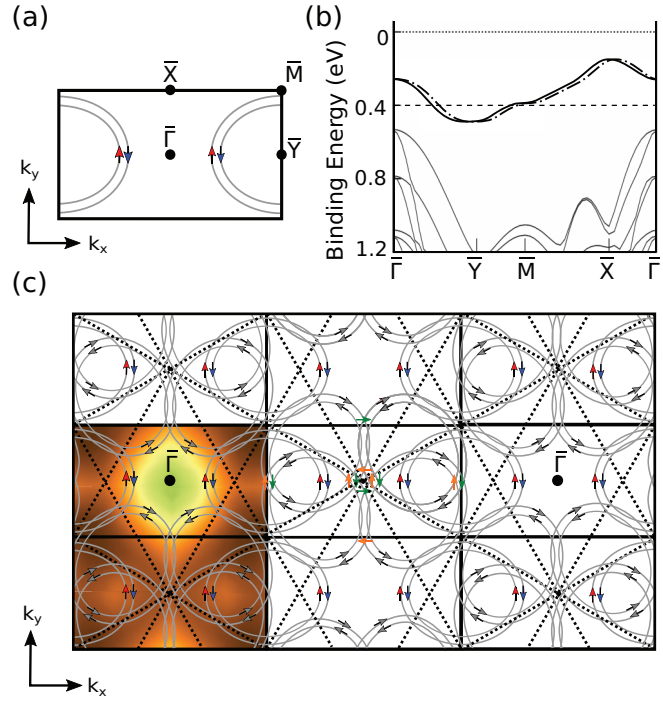

FIG. 7. (a) Electronic structure and spin texture in the SBZ of the $(2\sqrt{3} \times \sqrt{3})$ structure at a binding energy of 0.4 eV with a Rashba splitting of $\Delta k \approx 0.05$ Å^{-1}. (b) Band structure reproduced after Lee *et al.* [17]. The Mott state was complemented by Rashba splitting. (c) SBZs consisting of three rotational $(2\sqrt{3} \times \sqrt{3})$ domains. Red and blue spin vectors belong to the horizontal domain as seen in (a). Spin components of the other two domains are shown in gray, the resulting spins of those domains along the k_x and k_y direction in orange and green. The broad gray lines indicate the positions of measurements along the k_x and k_y direction shown in Fig. 3 and coincide with the lines denoted by (1) and (3) in Fig. 2(c).

spin polarization at these points with overlapping bands will depend on the distribution and size of the three domains.

IV. SUMMARY AND CONCLUSION

In summary, we investigated the spin-orbit interaction of the correlated α-Sn structure on Si(111) directly with spin- and angle-resolved photoemission. We were able to identify spin-resolved band structures which originate from a $(2\sqrt{3} \times \sqrt{3})$ symmetry, in agreement with previous theoretical studies [9,17]. This symmetry is mandatory for the formation of a row-wise collinear antiferromagnetically ordered spin arrangement of the Sn atoms adsorbed on T_4 positions with a $(\sqrt{3} \times \sqrt{3})$ order. As it turns out, the Rashba splitting is comparably small and the spin-orbit interaction is weak in this structure. According to the spin orientation in our ARPES experiments, we propose an in-plane ordering of the spins in the antiferromagnetic phase.

There is currently a debate whether the insulating state is driven by electronic correlation effects or by spin ordering [9,17]. In the latter case, where the ground state is characterized as a Slater-type insulator via band magnetism, the antiferromagnetic ordering should come along with a nesting in between helical states. However, a doubling of the unit

cell, as seen recently for Pb/Si(557) [15], was not observed. Moreover, we have not seen indications of hybridization between the Sn states and the Si valence bands ($3p_z$ states), which enables the superexchange. Therefore, we rather like to describe the α-Sn/Si(111) phase as a weakly spin-orbit coupled Mott system [12].

ACKNOWLEDGMENTS

We gratefully acknowledge the financial support by the Deutsche Forschungsgemeinschaft (project Te386/10-2 within the Research Unit FOR1700) and Swiss National Science Foundation (project PP00P2-144742).

[1] T. Zhang, P. Cheng, W.-J. Li, Y.-J. Sun, G. Wang, X.-G. Zhu, K. He, L. Wang, X. Ma, X. Chen, Y. Wang, Y. Liu, H.-Q. Lin, J.-F. Jia, and Q.-K. Xue, Nat. Phys. **6**, 104 (2010).

[2] B. Hafke, T. Frigge, T. Witte, B. Krenzer, J. Aulbach, J. Schäfer, R. Claessen, S. C. Erwin, and M. Horn-von Hoegen, Phys. Rev. B **94**, 161403 (2016).

[3] J. M. Carpinelli, H. H. Weitering, E. W. Plummer, and R. Stumpf, Nature (London) **381**, 398 (1996).

[4] I. Brihuega, O. Custance, R. Pérez, and J. M. Gómez-Rodríguez, Phys. Rev. Lett. **94**, 046101 (2005).

[5] C. Brun, T. Cren, V. Cherkez, F. Debontridder, S. Pons, D. Fokin, M. C. Tringides, S. Bozhko, L. B. Ioffe, B. L. Altshuler, and D. Roditchev, Nat. Phys. **10**, 444 (2014).

[6] J. Lobo, A. Tejeda, A. Mugarza, and E. G. Michel, Phys. Rev. B **68**, 235332 (2003).

[7] F. Ming, S. Johnston, D. Mulugeta, T. S. Smith, P. Vilmercati, G. Lee, T. A. Maier, P. C. Snijders, and H. H. Weitering, Phys. Rev. Lett. **119**, 266802 (2017).

[8] H. Morikawa, I. Matsuda, and S. Hasegawa, Phys. Rev. B **65**, 201308 (2002).

[9] G. Li, P. Höpfner, J. Schäfer, C. Blumenstein, S. Meyer, A. Bostwick, E. Rotenberg, R. Claessen, and W. Hanke, Nat. Commun. **4**, 1620 (2013).

[10] S. Modesti, L. Petaccia, G. Ceballos, I. Vobornik, G. Panaccione, G. Rossi, L. Ottaviano, R. Larciprete, S. Lizzit, and A. Goldoni, Phys. Rev. Lett. **98**, 126401 (2007).

[11] A. B. Odobescu, A. A. Maizlakh, N. I. Fedotov, and S. V. Zaitsev-Zotov, Phys. Rev. B **95**, 195151 (2017).

[12] W. Witczak-Krempa, G. Chen, Y. B. Kim, and L. Balents, Ann. Rev. Condens. Matter Phys. **5**, 57 (2013).

[13] P. Höpfner, J. Schäfer, A. Fleszar, J. H. Dil, B. Slomski, F. Meier, C. Loho, C. Blumenstein, L. Patthey, W. Hanke, and R. Claessen, Phys. Rev. Lett. **108**, 186801 (2012).

[14] S. Glass, G. Li, F. Adler, J. Aulbach, A. Fleszar, R. Thomale, W. Hanke, R. Claessen, and J. Schäfer, Phys. Rev. Lett. **114**, 247602 (2015).

[15] C. Brand, H. Pfnür, G. Landolt, S. Muff, J. H. Dil, T. Das, and C. Tegenkamp, Nat. Commun. **6**, 8118 (2015).

[16] C. Brand, S. Muff, M. Fanciulli, H. Pfnür, M. C. Tringides, J. H. Dil, and C. Tegenkamp, Phys. Rev. B **96**, 035432 (2017).

[17] J.-H. Lee, X.-Y. Ren, Y. Jia, and J.-H. Cho, Phys. Rev. B **90**, 125439 (2014), supplement.

[18] J.-H. Lee, H.-J. Kim, and J.-H. Cho, Phys. Rev. Lett. **111**, 106403 (2013).

[19] D. I. Badrtdinov, S. A. Nikolaev, M. I. Katsnelson, and V. V. Mazurenko, Phys. Rev. B **94**, 224418 (2016).

[20] M. Hoesch, T. Greber, V. N. Petrov, M. Muntwiler, M. Hengsberger, W. Auwaerter, and J. Osterwalder, J. Electron Spectrosc. Relat. Phenom. **124**, 263 (2002).

[21] F. Meier, J. H. Dil, and J. Osterwalder, New J. Phys. **11**, 125008 (2009).

[22] S. Heinze, M. Bode, A. Kubetzka, O. Pietzsch, X. Nie, S. Blügel, and R. Wiesendanger, Science **288**, 1805 (2000).